2472–2486 *Nucleic Acids Research, 2019, Vol. 47, No. 5* *Published online 11 February 2019*
doi: 10.1093/nar/gkz082

Loss of RNA-binding protein GRSF1 activates mTOR to elicit a proinflammatory transcriptional program

Ji Heon Noh[1,2,*,†], Kyoung Mi Kim[1,†], Poonam R. Pandey[1], Nicole Noren Hooten[3], Rachel Munk[1], Gautam Kundu[1], Supriyo De[1], Jennifer L. Martindale[1], Xiaoling Yang[1], Michele K. Evans[3], Kotb Abdelmohsen[1] and Myriam Gorospe[1,*]

[1]Laboratory of Genetics and Genomics, National Institute on Aging Intramural Research Program, National Institutes of Health, Baltimore, MD, USA, [2]Department of Biotechnology, Chonnam National University, Yeosu, Chonnam 59626, Republic of Korea and [3]Laboratory of Epidemiology and Population Science, National Institute on Aging Intramural Research Program, National Institutes of Health, Baltimore, MD, USA

Received November 07, 2018; Revised January 24, 2019; Editorial Decision January 29, 2019; Accepted January 31, 2019

ABSTRACT

The RNA-binding protein GRSF1 (G-rich RNA sequence-binding factor 1) critically maintains mitochondrial homeostasis. Accordingly, loss of GRSF1 impaired mitochondrial respiration and increased the levels of reactive oxygen species (ROS), triggering DNA damage, growth suppression, and a senescent phenotype characterized by elevated production and secretion of interleukin (IL)6. Here, we characterize the pathways that govern IL6 production in response to mitochondrial dysfunction in GRSF1-depleted cells. We report that loss of GRSF1 broadly altered protein expression programs, impairing the function of respiratory complexes I and IV. The rise in oxidative stress led to increased DNA damage and activation of mTOR, which in turn activated NF-κB to induce *IL6* gene transcription and orchestrate a pro-inflammatory program. Collectively, our results indicate that GRSF1 helps preserve mitochondrial homeostasis, in turn preventing oxidative DNA damage and the activation of mTOR and NF-κB, and suppressing a transcriptional pro-inflammatory program leading to increased IL6 production.

INTRODUCTION

RNA-binding proteins (RBPs) associate with coding and noncoding RNAs to perform a number of molecular functions in eukaryotic cells, some of them for the maintenance of cellular 'housekeeping' activities, others for the implementation of specific gene expression programs in response to certain signals (1). In the nucleus, RBPs influence gene transcription, precursor RNA splicing, as well as RNA maturation and export to the cytosol (1–3). In the cytoplasm, RBPs control RNA mobilization, storage, degradation, stabilization, modification, turnover, translation, and export to extracellular vesicles (1–3). By controlling these processes, RBPs modulate cell division, differentiation, quiescence, apoptosis, and responsiveness to stress and immune factors (4–8).

RBPs govern many of the cellular changes that occur as a result of advancing age, such as telomere shortening, epigenetic modifications, impaired responses to nutrient and damaging signals, loss of genomic integrity, and senescence (9–12). Associated with these changes is a progressive loss of mitochondrial function, another hallmark of aging cells (13,14). Mitochondrial activity, which is essential for generating energy (ATP), is controlled through gene expression programs driven by both nuclear DNA and mitochondrial (mt)DNA. In addition to producing energy, mitochondria influence cell metabolism by producing reactive oxygen species (ROS), regulating calcium levels in the cytosol, and modulating apoptosis (13,14). Given that these processes directly influence the function of tissues and organs, the decline in mitochondrial activity with age has been linked closely with age-related physiologic deterioration, particularly the reductions in strength, tissue regeneration, and immune function (13).

The RBP G-rich RNA sequence-binding factor 1 (GRSF1) is encoded by nuclear DNA, but following translation, its mitochondria-localization signal ensures its rapid mobilization to mitochondria (15,16). GRSF1 is an integral constituent of mitochondrial RNA granules, specialized ribonucleoprotein (RNP) complexes that also include the ribonuclease RNase P which cleaves precursor polycistronic mitochondrial RNAs and releases mRNAs and tRNAs (15,16). In addition, GRSF1 facilitates the loading of mature mRNA onto mitochondrial ribosomes (16). In-

*To whom correspondence should be addressed. Tel: +1 410 558 8443; Fax: +1 410 558 8331; Email: gorospem@grc.nia.nih.gov
Correspondence may also be addressed to Ji Heon Noh. Email: journi1117@gmail.com
†The authors wish it to be known that, in their opinion, the first two authors should be regarded as Joint First Authors.

terestingly, the interaction of GRSF1 with the long noncoding (lnc)RNA *RMRP* in the mitochondrial matrix retained *RMRP* in mitochondria and enhanced mitochondrial oxidative phosphorylation (17). These studies provided molecular evidence that GRSF1 RNPs are critical regulators of mitochondrial function.

We recently reported that the DNA damage and impaired cell proliferation seen in cells in which GRSF1 was depleted mirrored the phenotype of senescent cells (18), supporting the view that GRSF1 prevented premature senescence by preserving mitochondrial function. Accordingly, GRSF1-depleted cells were growth arrested, displayed senescence markers such as cyclin-dependent kinase inhibitors (p21 and p16) and a senescence-associated β-galactosidase activity (18). Importantly, GRSF1 depletion also led to the production of a pivotal senescence-associated factor, the pro-inflammatory cytokine interleukin (IL)6. Here, we set out to investigate how mitochondrial dysfunction resulting from loss of GRSF1 led to the production of IL6. Our findings indicate that GRSF1 deficiency profoundly modified protein expression programs in human embryonic kidney (HEK) 293 fibroblasts, impairing the function of mitochondrial complexes I and IV. The ensuing oxidative stress led to extensive DNA damage and the activation of mammalian target of rapamycin (mTOR). The major mTOR target nuclear factor kappa B (NF-κB) in turn induced the transcription of the *IL6* gene and contributed to implementing a pro-inflammatory transcriptional program.

MATERIALS AND METHODS

Cell culture, transfection, transduction, and treatment

HEK293 cells were cultured in Dulbecco's modified Eagle's medium (DMEM) supplemented with 10% fetal bovine serum (FBS, Gibco), and antibiotics and antimycotics (Invitrogen), and were counted using a TC-20 cell counter (Bio-Rad). Cells were transfected with 50 nM of control siRNA (siCTRL) or siRNAs targeting mTOR, NF-κB1 or RelA using Lipofectamine 2000 (Thermo Fisher Scientific). Lentiviral particles delivering either GRSF1-specific (TL312593V, OriGene) or scrambled control (TR30021V, OriGene) shRNA were transduced into HEK293 cells in the presence of 8 μg/mL of Polybrene with a MOI (Multiplicity of infection) of 20. Three days after transduction cells were maintained in culture media supplemented with 3 μg/mL of Puromycin (Santa Cruz Biotechnology). Rapamycin (R8781, Sigma) was added into the culture medium of HEK293 cells (25 or 50 nM).

HEK293 cells stably expressing RelA (LR-7008)- or IL-6 (SL-0048-NP)-responsive luciferase reporter were purchased (Signosis), and the luciferase activity was determined by Dual-Luciferase® reporter assay system according to the manufacturer's instruction (Promega).

Western blot analysis

Cells were lysed in lysis buffer containing one of two different detergents, NP-40 (50 mM Tris–Cl [pH 7.5], 150 mM NaCl, 1 mM $MgCl_2$ and 1% NP-40) or Triton X-100 (50 mM HEPES [pH 7.4], 5 mM EDTA, 50 mM NaCl and 1% Triton X-100) supplemented with 1 mM PMSF and a protease and phosphatase inhibitor cocktail (Thermo Fisher Scientific). Cytoplasmic and nuclear fractions were prepared using NE-PER extraction reagents (Thermo Fisher Scientific) according to the manufacturer's instructions. The purity of each fraction was assessed by immunoblotting using antibodies that recognized predominantly nuclear (HDAC and NF90) or cytoplasmic (GAPDH) proteins.

Proteins were subjected to PAGE using 4–12% NuPAGE or 6% Tris-glycine gel, transferred onto nitrocellulose membranes (iBlot Stack, Thermo Fisher Scientific), and incubated with primary antibodies: GRSF1 (AV40382) from Sigma; p16 (551154) and NF90 (612155) from BD Biosciences; β-Actin (sc-47778), HSP90 (sc-1055), p53 (sc-126), GAPDH (sc-32233), HuR (sc-5261), HDAC2 (sc-7899), PNPASE (sc-271479) and NF-κB(p65) (sc-109), CHK2 (sc-17747) from Santa Cruz Biotechnology; p21 (05–345) from Millipore; p-STAT3(S727) (#9136), p-mTOR(S2448) (#5536), mTOR (#2972 and #2983), p-4E-BP1(S65) (#9451), 4E-BP1 (#9452), p-S6(S240/244) (#5364), p-ERK(T202/Y204) (#9101), S6K (#9202) and NF-κB1(p50/p105) (#13586) from Cell Signaling; IL6 (AF-206-NA) from Thermo Fisher Scientific; and p-S6K(T389) (ab32359) from Abcam. After incubation with secondary antibodies (GE Healthcare), Western blotting signals were detected by enhanced chemiluminescence (Millipore) using a KwikQuant Imager (Kindle Biosciences, LLC).

[^{3}H]-Thymidine incorporation assay

HEK293 cells expressing lentiviral shRNAs (shGRSF1 or shCTRL) were cultured in six-well plates and incubated with 1 μCi/ml of [^{3}H]-thymidine (Perkin Elmer) for 16 h at 37°C, whereupon cells were washed twice with ice-cold PBS, washed twice with 5% TCA, and solubilized in 0.8 ml lysis buffer (0.5 M NaOH, 2% SDS). The solubilized cell suspension (0.4 ml) was collected into vials containing 5 ml of scintillation cocktail and the radioactivity was measured using LS6500 scintillation counter (Beckman). Data were normalized to total protein amounts used for each sample.

Antibody arrays

Multiple cytokines and chemokines were detected using RayBio™ Human Cytokine Array (Raybiotech). Briefly, collected conditioned media were incubated with antibody-blotted membrane at 4°C for 16 h, biotinylated antibody at 4°C for 16 h, and streptavidin-HRP for 2 h at 25°C. Signals were detected using enhanced Chemiluminescence (Raybiotech). Protein phosphorylation in whole-cell lysates was assessed using the Human Phospho-Kinase Array Kit (Proteome Profiler, R&D systems) following the manufacturer's instructions.

Measurement of secreted IL6

The AlphaLISA® Human Interleukin-6 (IL6) Detection Kit (Perkin Elmer Inc.) was used to measure IL6 in conditioned media (CM) according to the manufacturer's instructions. To prepare CM, cells were cultured in serum-depleted media for 18 h, unless indicated. IL6 levels were normalized to cell numbers in the population.

Reverse transcription (RT) and real-time quantitative (q)PCR analysis

Total RNA was extracted using TriPure Isolation Reagent (Roche), and cDNA was synthesized using random hexamers and reverse transcriptase (Invitrogen). Gene-specific primers were then used for qPCR amplification by employing SYBR Green master mix (Kapa Biosystems) and an Applied Biosystems 7300 instrument. Primer sequences are as follows (forward [F] and reverse [R], respectively):

- IL1A_F 5′-GGTTGAGTTTAAGCCAATCCA; IL1A_R 5′-TGCTGACCTAGGCTTGATGA
- IL1B_F 5′-CTGTCCTGCGTGTTGAAAGA; IL1B_R 5′-TTGGGTAATTTTTGGGATCTACA
- IL6_F 5′-GCCCAGCTATGAACTCCTTCT; IL6_R 5′-GAAGGCAGCAGGCAACAC
- IL6 pre_2F 5′-AGGAGACTTGCCTGGTGAAA; IL6 pre_2R 5′-CCAAGTTGAGGGAATGAGGA
- IL8_F 5′-GAGTGGACCACACTGCGCCA; IL8_R 5′-TCCACAACCCTCTGCACCCAGT
- P16_F 5′-GCACCGAATAGTTACGGTCGG; p16_R 5′-CACCAGCGTGTCCAGGAAGC
- P21_F 5′-CCTGCCCAAGCTCTACCTT; P21_R 5′-AAGGCAGAAGATGTAGAGC
- CCL13_F 5′-ACCTTCAACATGAAAGTCTCTGC; CCL13_R 5′-GGACGTTGAGTGCATCTGG
- GAPDH_F 5′-TGCACCACCAACTGCTTAGC; GAPDH_R 5′-GGCATGGACTGTGGTCATGAG
- ACTIN_F 5′-CATGTACGTTGCTATCCAGGC; ACTIN_R 5′-CTCCTTAATGTCACGCACGAT
- 18S rRNA_F 5′-CGAACGTCTGCCCTATCAACTT; 18S rRNA_R 5′-ACCCGTGGTCACCATGG
- IL12A_F 5′- GCTCCAGAAGGCCAGACAAA; IL12A_R 5′- GCCAGGCAACTCCCATTAGT
- IGFBP3_F 5′-CAGAGACTCGAGCACAGCAC; IGFBP3_R 5′-GATGACCGGGGTTTAAAGGT
- MCP1_F 5′-CCCCAGTCACCTGCTGTTAT; MCP1_R 5′-AGATCTCCTTGGCCACAATG
- ANG_F 5′-GGGGTTTTGTTGTTGGTCTT; ANG_R 5′-AGTGCTGGGTCAGGAAGTGT
- MIF_F 5′-AGAACCGCTCCTACAGCAAG; MIF_R 5′-CAGTTGTTCCAGCCCACATT

Measurement of mitochondrial activity

OCR (oxygen consumption rate) and ECAR (extracellular acidification rate) measurement were performed using XF24 Extracellular Flux analyzer (Seahorse Bioscience) as previously described (17). Basal OCR and ECAR were reported as absolute rates (pmol/min for OCR and mpH/min for ECAR) and normalized by counted cell number.

The activities of complexes I and IV were measured using microplate assay kits (Abcam) according to the manufacturer's instructions. For complex I, normalized protein lysates were loaded onto the immunocapture plate and incubated for 3 h at 25°C. After washing, the oxidation of NADH into NAD+ was determined by measuring the coupled dye reduction at 450 nm. For measuring complex IV activity, diluted proteins were loaded onto the plate for immunocapturing. After washing, cytochrome *c* was added, and its oxidation rate was determined by measuring the decline of absorbance at 550 nm.

NAD^+ and NADH levels were determined by using an NAD^+/NADH quantification kit (MAK037; Sigma-Aldrich) following the manufacturer's instructions. Briefly, 2×10^5 cells were homogenized in 400 μl of extraction buffer and clarified at 13 000 × g for 10 min at 4°C. Total levels of NADH plus NAD (NAD_{total}) or NADH only were measured separately. To measure NADH only, NAD was decomposed by heating at 60°C for 30 min. NADH standards (20–100 pmol/well) were used for quantification. Similarly, total NADP or NADPH only was also measured using NADP/NADPH quantitation kit (MAK038; Sigma-Aldrich) following the manufacturer's instructions.

ROS measurement

The level of intracellular reactive oxygen species (ROS) was measured by using a DCFDA (2′,7′-dichlorodihydrofluorescein diacetate) cellular ROS detection assay kit (Abcam) following the manufacturer's instructions. Briefly, GRSF1-deficient or wild-type HEK293 cells were plated at 2×10^4 cells/well on 96-well plates (black/clear bottom, PerkinElmer) and cultured overnight in complete DMEM without phenol red (Life Technologies) at 37°C with 5% CO_2. Cells that reached ∼80% confluence were washed and incubated with 20 μM DCFDA in phenol red-free DMEM at 37°C for 45 min. Fluorescence intensity was read at 485/535 nm (excitation/emission) by using a VICTOR3 microplate reader (PerkinElmer).

Polysome analysis

Polysome analysis was performed as previously described (19). Briefly, cells were treated with cycloheximide (Calbiochem; 100 μg/ml) for 10 min and lysed in PEB (polysome extraction buffer; 20 mM Tris–HCl [pH 7.5], 100 mM NaCl, 5 mM $MgCl_2$ and 0.3% NP-40). After the lysate was separated through 10–50% sucrose gradients, 12 fractions were collected for further analysis. The distribution of mRNAs was quantified by RT-qPCR analysis and plotted as a percentage of the specific mRNA in each fraction relative to the total amount of that mRNA in the gradient.

Comet assay

The alkaline comet assay was performed as previously described (20). The comets were visualized using an Eclipse E-400 fluorescence microscope (Nikon, Japan) attached to a Pulnix video camera (Kinetic Imaging, LTD, Liverpool, UK) and analyzed using Komet 5.5 software (Kinetic Imaging Ltd). Olive tail moment (OTM) values served as a measure of the extent of DNA damage; 50 cells were counted per condition. Similar results were obtained when % tail DNA was examined.

NF-κB p65 transcription factor activity

NF-κB activation was assessed using NF-κB p65 Transcription Factor Assay Kit (ab133112; Abcam) following

the manufacturer's instructions. In brief, nuclear fractions were isolated from GRSF1 KO and WT HEK293 cells transfected with either siMTOR or siCTRL and loaded into wells containing an immobilized NF-κB consensus sequence (RHD [Rel-like] domain) and incubated overnight at 4°C. An antibody recognizing NF-κB p65 was loaded into each well and incubated at 25°C for 1 h; after washing, samples were incubated with the HRP-conjugated secondary antibody at 25°C for 1 h. To quantify transcription factor binding, a developing solution was added to each well and incubated at 25°C for 15–45 min. Signals were quantified using a VICTOR3 microplate reader (Perkin Elmer) with absorbance at 450 nm.

Quantification of nascent transcription

Nascent mRNA was quantified as previously described (17) with a few modifications. Briefly, HEK293 cells stably expressing shGRSF1 (or shCTRL) were cultured in media containing 4-thiouridine (4-SU, 100 μM, Sigma) and the nascent RNA was metabolically labeled for up to 2 h. Total RNA (50 μg) was biotinylated in a labeling reaction including 30 μl of Biotin-HPDP (Pierce) dissolved in 1 mg/mL dimethylformamide (DMF, Sigma) and 20 μl of 10 × biotinylation buffer (100 mM Tris–HCl, pH 7.4, 10 mM EDTA) at 25°C for 1.5 h. Biotinylated RNA was then purified using chloroform/isoamylalcohol (24:1) extraction, and the RNA pellet was resuspended in 100 μl of RNase-free water with 0.1 mM EDTA. The labeled RNA was then heated (65°C, 5 min), chilled on ice briefly, and incubated with 100 μl of streptavidin beads (Miltenyi Biotec) with rotation for 20 min. Beads were loaded onto the equilibrated μMacs columns (Miltenyi Biotec), and washed with washing buffer (100 mM Tris–HCl, pH7.5, 10 mM EDTA, 1 M NaCl and 0.1% Tween-20) three times each. Captured RNA was then eluted directly using 700 μl of RLT buffer (Qiagen) using 100 μl of dithiothreitol (DTT, 100 mM) twice. Eluted nascent RNA was recovered using RNeasy MinElute spin columns (Qiagen) following the manufacturer's instruction and measured by RT-qPCR analysis.

Proteomic analysis (iTRAQ) and quantification

iTRAQ based proteomic analysis was performed. Briefly, four samples (whole-cell lysates from two wild-type [WT] and two GRSF1 knockout [KO] cell lines) were lysed in a lysis buffer (8 M urea, 50 mM HEPES [pH 8.5]). After centrifugation at 20,000 g and 4°C for 60 min, the protein concentration of the supernatant was determined using BCA assay (Thermo Fisher Scientific). The protein disulfide bonds in the supernatant were reduced for 40 min with 5 mM dithiothreitol at RT and alkylated for 40 min with 15 mM iodoacetamide in the dark. Alkylated protein samples were diluted with 100 mM HEPES pH 8.5 to 2 M urea followed by digestion overnight at 37°C with trypsin in a 1:50 enzyme-to-substrate ratio (Promega, V5113). After digestion, the peptide mixtures were acidified with trifluoroacetic acid (TFA) to 1%, and subjected to C18 solid-phase extraction (Empore, 3M). Finally, the desalted peptide samples were dried in a vacuum concentrator and stored at −20°C for peptide TMT (tandem mass tag) labeling.

The desalted peptides were dissolved in 100 μl of 100 mM TEAB, pH 8.5. The peptide concentration was measured using a MicroBCA assay (Thermo Fisher Scientific), and 100 μg of digested peptides were incubated with 42 μl TMT reagents (Thermo Fisher Scientific) for 1 h at room temperature. Reactions were quenched by adding 8 μl of 5% hydroxylamine and incubating for 15 min. TMT-labeled samples were combined at a 1:1:1:1 ratio according to the sample information table, desalted using Sep-Pak C18 cartridges, and dissolved in 20 mM NH_4FA, pH 10. The peptide mixtures were loaded into a home-made Stagetip-based high pH reverse phase fraction method. A total of seven peptide fractions were obtained, acidified using 1% TFA, and desalted prior to LC–MS/MS analysis.

The dried peptides were dissolved in 20 μl of 0.2% formic acid and subjected to nano LC–MS/MS analysis. The peptides were separated with the home-made C18 reverse-phase column packed with 15 cm of ReproSil-Pur C18-AQ resin (3 μm, 120 Å, Dr Maisch GmbH, Ammerbuch, Germany). Peptides were eluted with a 2 h gradient of 6–30% acetonitrile in 0.1% formic acid at a flow rate of 300 nl/min using an Easy nLC 1000 system (Thermo Fisher Scientific). The eluted peptides were analyzed directly with an Q Exactive MS (Thermo Fisher Scientific). The spray voltage was set to 2.0 kV. Full-scan MS survey spectra (m/z 300–1600) in profile mode were acquired in the Orbitrap with a resolution of 30 000 after accumulation of 1 000 000 ions, followed by four CID fragmentation (collision-induced dissociation; normalized collision energy, 35%; activation time 30 ms, isolation width 1.0 m/z) and four HCD fragmentation (higher-energy collisional dissociation, normalized collision energy 70%, maximum inject time 300 ms; mass resolution, 7500; activation time 30 ms) for the four most intense peptide ions selected from the survey scan in the Orbitrap.

A total of eight raw MS files (5–1 to 5–8) were processed with Proteome Discoverer (Version 1.4, Thermo Fisher Scientific) and searched against Uniprot Human protein sequence database. The parameters were set as follows: fixed modifications, carbamidomethylation (C), TMT/+229D-K and TMT/+229D-N terminal; oxidation (M) (variable); the enzyme specificity was set to trypsin; the maximum missed cleavages were set to 2; the precursor ion mass tolerance was set to 10 ppm, and MS/MS tolerance was 0.5 Da. The false positive rate (FDR) was set as 0.01. A TMT 6-plex quantitation method in Proteome Discoverer was applied for HCD-based peptide quantitation.

Two biological repeats were analyzed for each cell line (WT and KO), and the average ratio (KO relative to WT) was calculated using individual peptide ratios for each peptide. Differentially expressed proteins in mitochondria served as the starting point for subsequent experimental analysis.

Transcriptomic analysis

Global gene expression profiling covering both protein-coding genes and lncRNAs was performed and analyzed using the Arraystar microarray platform (Human 8 × 60K LncRNA expression array; Arraystar Inc.). Transcriptomic analysis was performed using the Agilent Feature Extraction software (version 11.0.1.1) for microarray im-

ages. Quantile normalization and subsequent data processing were performed using the GeneSpring GX v11.5.1 software package (Agilent Technologies). After quantile normalization of the raw data, mRNAs with flags in Present or Marginal ('All Targets Value') values in at least three out of six samples were chosen for further data analysis. Those mRNAs that were differentially expressed with statistical significance between the two groups were identified through Volcano Plot filtering. The thresholds were set as Fold Change $\geq$2.0 and *P*-value $\leq$0.05. Pathway and GO analyses were performed to determine the possible roles that the differentially expressed mRNAs played in specific biological pathways, and Hierarchical Clustering was performed to identify mRNA expression patterns among samples.

Statistical analysis

The statistical analysis of significance (*P*-value) was performed using two-tailed, unpaired *t*-test by using a web-based *t*-test calculator (GraphPad software). Values were represented as the means ± standard deviation.

RESULTS

Loss of GRSF1 increases oxidant-induced DNA damage and suppresses cell proliferation

We investigated the impact of ablating GRSF1 by examining three clonal lines (KO-1, KO-2, KO-3) derived from HEK293 cells in which the *GRSF1* gene was knocked out (KO) by CRISPR/Cas9-mediated gene editing (17), as confirmed by western blot analysis (Figure 1A). Compared with HEK293 WT cells, loss of GRSF1 reduced the proliferation of all GRSF1 KO clones (Figure 1B) and delayed cell cycle progression (Supplementary Figure S1). The impaired population growth was associated with increased DNA damage in HEK293 cells, as assessed by the alkaline comet assay. As shown, GRSF1 KO HEK293 clonal populations showed significantly higher Olive tail moment (OTM) values, indicating greater baseline DNA damage compared with HEK293 cells expressing normal GRSF1 levels (WT) (Figure 1C). Additionally, depleting GRSF1 elevated DNA damage response (DDR) proteins TP53 (p53) and the cyclin-dependent kinase (CDK) inhibitor CDKN1A (p21) (Figure 1D). Importantly, pre-treatment for 2 h with NAC (N-Acetylcysteine), a thiol-containing antioxidant, reduced significantly the DNA damage seen in KO cells (Figure 1E), indicating that GRSF1 critically prevents oxidant-generated DNA damage. Similarly, ectopic re-expression of GRSF1 reduced DNA damage, as determined by quantification of OTM values (Figure 1E) and by observing DNA damage 'comets' in cells (Figure 1F) from which OTMs were calculated, even if the DDR protein p21 remained elevated under these conditions (Figure 1G). Finally, DNA damage, as measured by monitoring OTM values and DDR markers, also increased robustly in HEK293 cells after silencing GRSF1 following infection with shGRSF1 lentivirus compared with control cells infected with shCTRL. This effect was seen when assessing both pool shGRSF1 populations (Figure 1H) and individual shGRSF1 clones (Figure 1I). As observed in GRSF1 KO cells (Figure 1B), cell proliferation was also suppressed when GRSF1 was silenced (Figure 1J). These findings indicate that loss of GRSF1 promotes DNA damage and reduces cell division.

GRSF1 is essential for maintaining oxidative phosphorylation and mitochondrial complex I activity

To gain insight into how GRSF1 influenced oxidative DNA damage and cell proliferation, we investigated global protein expression programs by iTRAQ mass spectrometry (MS) analysis. After iTRAQ labeling of WT and KO cells (Materials and Methods), mitochondrial proteins differentially expressed were identified and served as the starting point for subsequent experimental analysis. As shown (Figure 2A and Supplementary Table S1), KO cells expressed reduced levels of many mitochondria-directed proteins; the levels of mtDNA-encoded proteins MT-COX2, MT-ATP6, and MT-ATP8 were displayed separately (Figure 2B). Interestingly, many of the mitochondria-directed proteins most markedly reduced in KO cells were components of mitochondrial Complexes I and IV (Figure 2A). To study if these gene expression patterns were consistent with altered glycolysis, we measured oxygen consumption and extracellular acidification rates (OCR/ECAR) in HEK293 GRSF1 KO cells. Loss of GRSF1 resulted in increased glycolysis, as OCR/ECAR ratios were lower in KO cells (three clones) compared to WT cells (Figure 2C). Complex I activity in HEK293 cells declined robustly after silencing GRSF1 following infection with shGRSF1 lentivirus compared with control cells infected with shCTRL (Figure 2D), while Complex IV activity, as determined by measuring cytochrome *c* oxidation, only declined modestly (Figure 2E). Complex I is a major source of superoxide anion (O_2^-) (21); using DCFDA, which detects hydroxyl and peroxyl radicals derived from superoxide, we found higher ROS levels in KO than WT HEK293 cells (Figure 2F). Analysis of NAD+/NADH ratios revealed a redox balance in favor of NAD+ in WT compared with KO HEK293 cells (Figure 2G), while the lower NADP+/NADPH ratios in HEK293 KO cells indicated that the cellular ROS scavenging activity is likely impaired in the KO cells (Figure 2H). These results indicate that ablating GRSF1 disrupts the balance in NAD+/NADH and NADP+/NADPH levels.

These findings indicate that GRSF1 ensures the proper levels of mitochondria-resident proteins essential for the activity of Complexes I and IV, thereby enabling optimal respiration. By reducing the function of Complexes I and IV, the loss of GRSF1 raised mitochondria-derived ROS, impaired oxidative phosphorylation, lowered the cell's reducing potential and lowered NAD+/NADH and NADP+/NADPH ratios, together contributing to cellular stress. These results further indicate that GRSF1 is essential for preventing ROS-generated DNA damage, as well as for maintaining mitochondrial OX-PHOS activity.

GRSF1 increases the production of cytokines, particularly IL6

We further delineated the impact of GRSF1 loss on cell signaling by identifying kinase cascades differentially

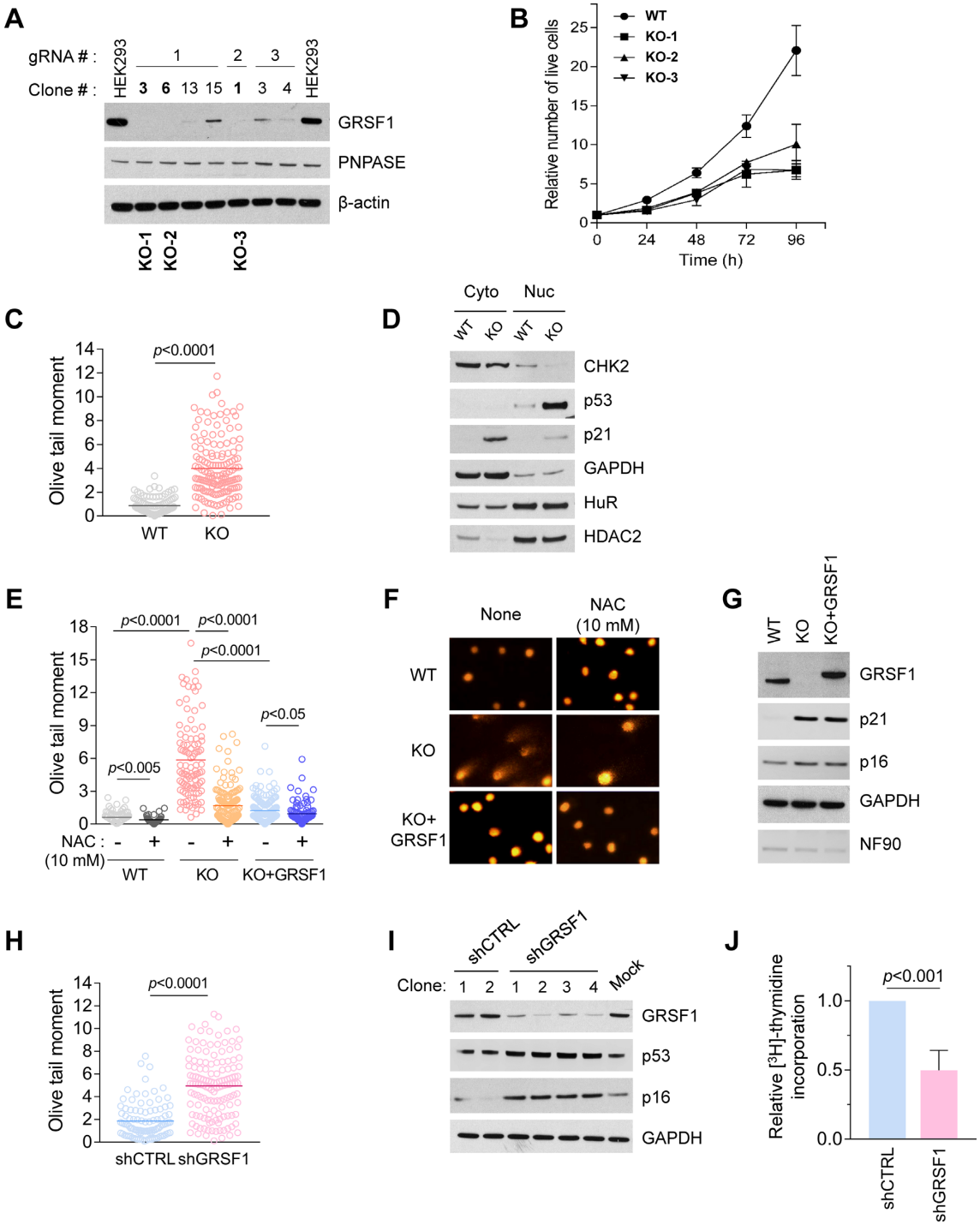

Figure 1. GRSF1 ablation increases DNA damage, reduces cell proliferation. (**A**) GRSF1 was ablated in HEK293 cells via CRISPR-Cas9-mediated gene editing using three different gRNAs (#1, #2, #3). The GRSF1 KO clones selected (KO-1, KO-2, KO-3) are indicated (bold). The expression of GRSF1 and loading controls PNPASE and β-Actin was assessed by Western blot analysis. (**B**) The growth of WT, KO-1, KO-2, and KO-3 populations was monitored by counting the number of viable cells. (**C**, **D**) Constitutive DNA damage was assessed in WT and KO HEK293 cells by the alkaline comet assay and quantified by measuring OTM values (C), and the levels of several DDR proteins in the cell populations were assessed by western blot analysis in nuclear (Nuc) and cytoplasmic (Cyto) lysates (D). GAPDH and HDAC2 were included as cytoplasmic and nuclear markers, respectively; GAPDH and HuR served as loading controls. (**E–G**) DNA damage was assessed in WT, KO or KO+GRSF1 HEK293 with or without treatment with NAC (10 mM, 2 h) by the alkaline comet assay, as described in panel C (E,F), and by Western blot analysis of cytoplasmic lysates, as described in panel D (G). (**H–J**) DNA damage was assessed in constitutively silenced pool populations of shCTRL and shGRSF1 cells by the alkaline comet assay and quantified by measuring OTM values (H), the levels of DDR proteins were assessed by Western blot analysis (I), and cell proliferation was assessed by monitoring [^{3}H]-thymidine incorporation (J). The data in (B,J) represent the means ±S.D. from three independent experiments.

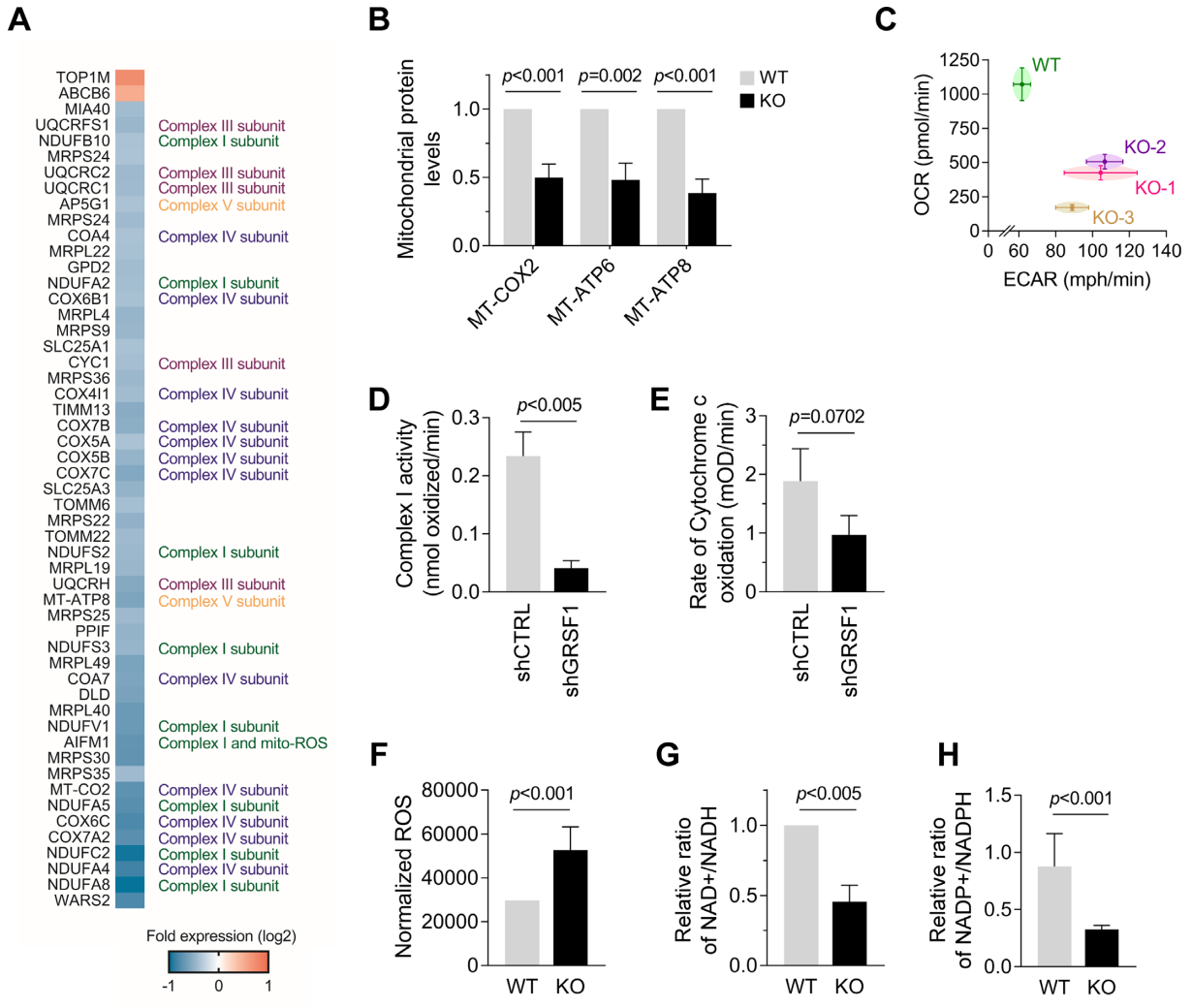

Figure 2. GRSF1 loss alters protein expression programs and impairs respiratory complexes I and IV. (**A**) iTRAQ-based quantitative proteomic analysis of the global response to GRSF1 depletion in two HEK293 KO clones relative to WT cells (Materials and Methods). A heat map of the relative abundance of proteins (log2 ratio) was generated from the iTRAQ-derived quantifications. (**B**) The levels of mitochondrial (MT) proteins COX2, ATP6, and ATP8 were assessed from the mass spec analysis. (**C**) Basal OCR and ECAR of three GRSF1 KO clonal cells (KO-1, 2 and 3) and parental HEK293 cells (WT) were measured using an extracellular flux (XF) analyzer. (**D–H**) The enzyme activities of the mitochondrial complex I (D) and IV (E) were analyzed in HEK293 cells stably expressing shGRSF1 or shCTRL; the cellular levels of ROS were measured with the use of a general ROS indicator CM-H2DCFDA (F), and the relative levels of NAD+/NADH (G) and NADP+/NADPH (H) ratios were determined in WT and KO HEK293 cells. The data in (B–H) are the means and ±SD of three independent experiments.

active in WT and KO HEK293 cells using antibody arrays to study protein phosphorylation. WT and KO cells were serum-starved for 18 h (recipient cells) and treated with conditioned medium (CM) collected from WT or KO HEK293 cells as indicated (Figure 3A). The screen revealed higher phosphorylation of STAT proteins, including p-STAT3(Y705), in GRSF1 KO cells that were cultured in KO CM, but not in WT CM. Similarly, mTOR signaling (TORC1) was activated [p-mTOR(S2448), p-S6K(T389), and p-S6K(T421/S424)] in GRSF1 KO cells treated with KO CM, although the level of p-S6K(T389) in GRSF1 KO cells was higher regardless of CM used. Signals corresponding to phosphorylated S6K(T389), S6K(T421/S424), STAT3(Y705), and mTOR(2448) are shown in Supplementary Figure S2. Silencing GRSF1 transiently by infection with a lentivirus that expressed shGRSF1 similarly increased the phosphorylation of S6K(T389), mTOR(S2448), and ERK (T202/Y204) (Figure 3B). Given the direct implication of mTOR, S6K, and STAT3 in the production and secretion of cytokines, chemokines, growth factors, and angiogenic factors (22–25), we assessed the production of these factors in CM in cells with normal or reduced GRSF1 levels using cytokine arrays (Figure 3C); a sample array is shown on the left, quantification on the signals on the right (*graph*). The levels of the cytokine most prominently upregulated in CM from shGRSF1 cells, IL6, were measured by the highly sensitive assay AlphaLISA (Figure 3D).

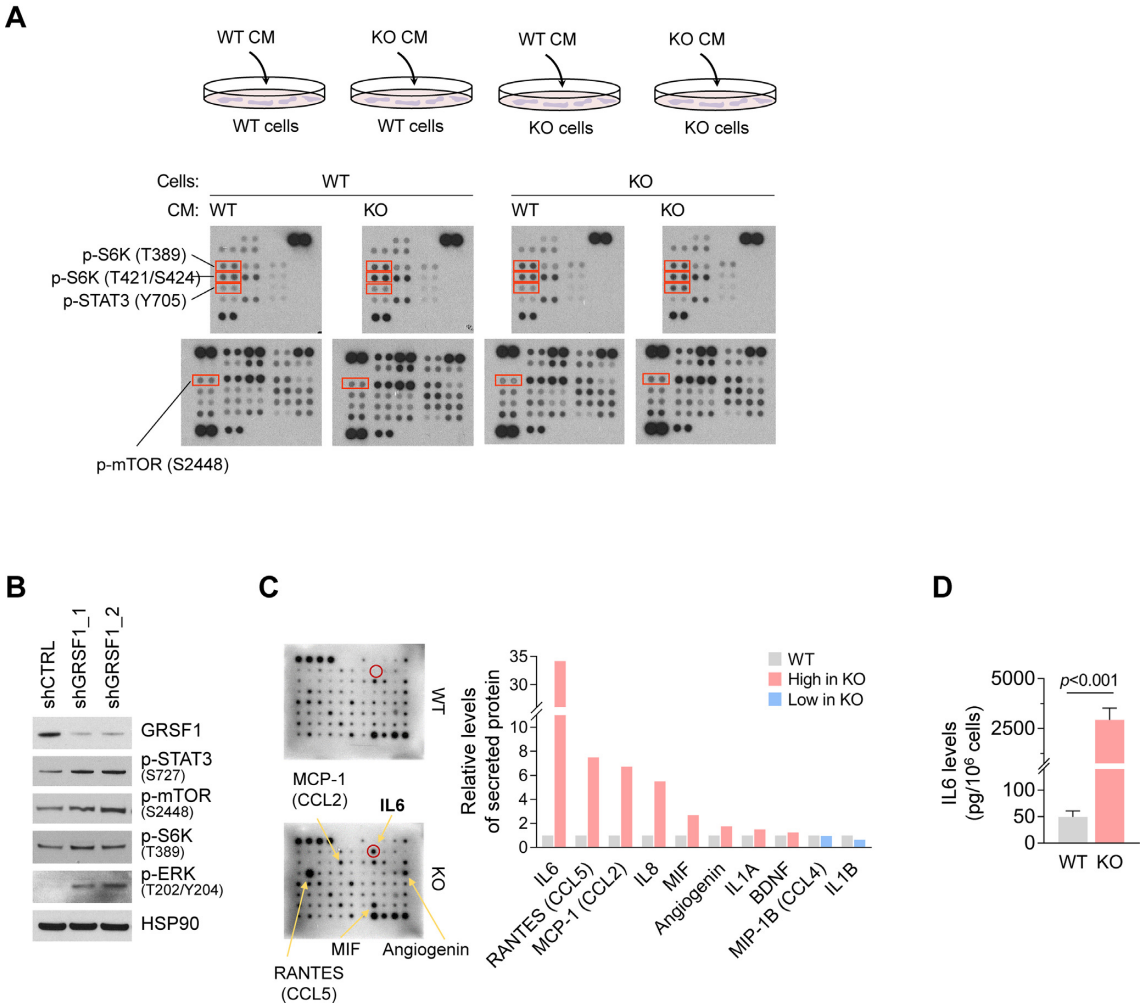

Figure 3. Silencing GRSF1 increases production of cytokines including IL6. (**A**) WT and KO HEK293 cells were cultured in conditioned media (CM) prepared from either WT or KO cells; 48 h later, whole-cell lysates (WCL) were prepared and subsets of phosphorylated proteins were assessed by using antibody arrays and quantified (Supplementary Figure S2). (**B**) The increase in phosphorylated STAT3, mTOR, S6K, and ERK was validated by Western blot analysis in HEK293 cells expressing normal GRSF1 levels (shCTRL) as well as in two clones of constitutively silenced GRSF1 (shGRSF1_1 and shGRSF1_2). (**C**) CM was collected from WT and KO cells, analyzed by antibody arrays (*left*), and the levels of secreted proteins were quantified (*right*). (**D**) Secreted IL6 levels in WT and KO HEK293 cells were quantified by AlphaLISA. The data in (A–C) are representative from two independent experiments. The data in (D) represent the means ± SD from three independent experiments.

Elevation of IL6 production is induced by the mTOR/NF-κB regulatory axis

To test if mTOR activation influenced the rise in IL6 secretion, GRSF1-deficient HEK293 cells were transfected with vectors expressing constitutively active (CA)- or wild-type (WT)-mTOR in the presence of Rapamycin (which inhibits S6K phosphorylation [p-S6K(T389)]); WT cells did not exhibit this response (not shown). As determined by Western blot and cytokine array analyses, in the presence of CA-mTOR, GRSF1 KO cells secreted elevated levels of IL6, as well as other factors like Angiogenin and CCL1 (Figure 4A and B). Intriguingly, RT-qPCR analysis revealed that among the mRNAs induced by mTOR activation, *IL6* mRNA levels increased most robustly (2- to 3-fold; Figure 4C). Conversely, siRNA-mediated mTOR silencing significantly reduced the production of *IL1A*, *IL1B* and *IL6* mRNAs that were highly expressed in KO relative to WT HEK293 cells (Figure 4D and E). These data indicate that the activated mTOR signaling might contribute to triggering *IL6* gene transcription.

In agreement with the transcriptional regulation of cytokines by mTOR/NF-κB (26), silencing mTOR significantly reduced the active NF-κB p65/RelA that was elevated in GRSF1 KO cells (KO), suggesting that the cytokine genes induced by GRSF1 depletion may be regulated transcriptionally by NF-κB (Figure 5A). The augmentation of NF-κB-driven transcription in GRSF1-depleted cells (shGRSF1) was further validated by employing HEK293 cells stably transfected with a luciferase reporter gene under the control of an NF-κB p65/RelA-responsive element (Figure 5B), further indicating that ablating GRSF1 increased NF-κB (p65)-mediated transcription. Moreover, while the levels of NF-κB target transcripts *IL6*, *IL8*, *IL1A* and *IL1B* mRNAs, which encode the major inflammatory cytokines that comprise the so called 'IL1-arm', were

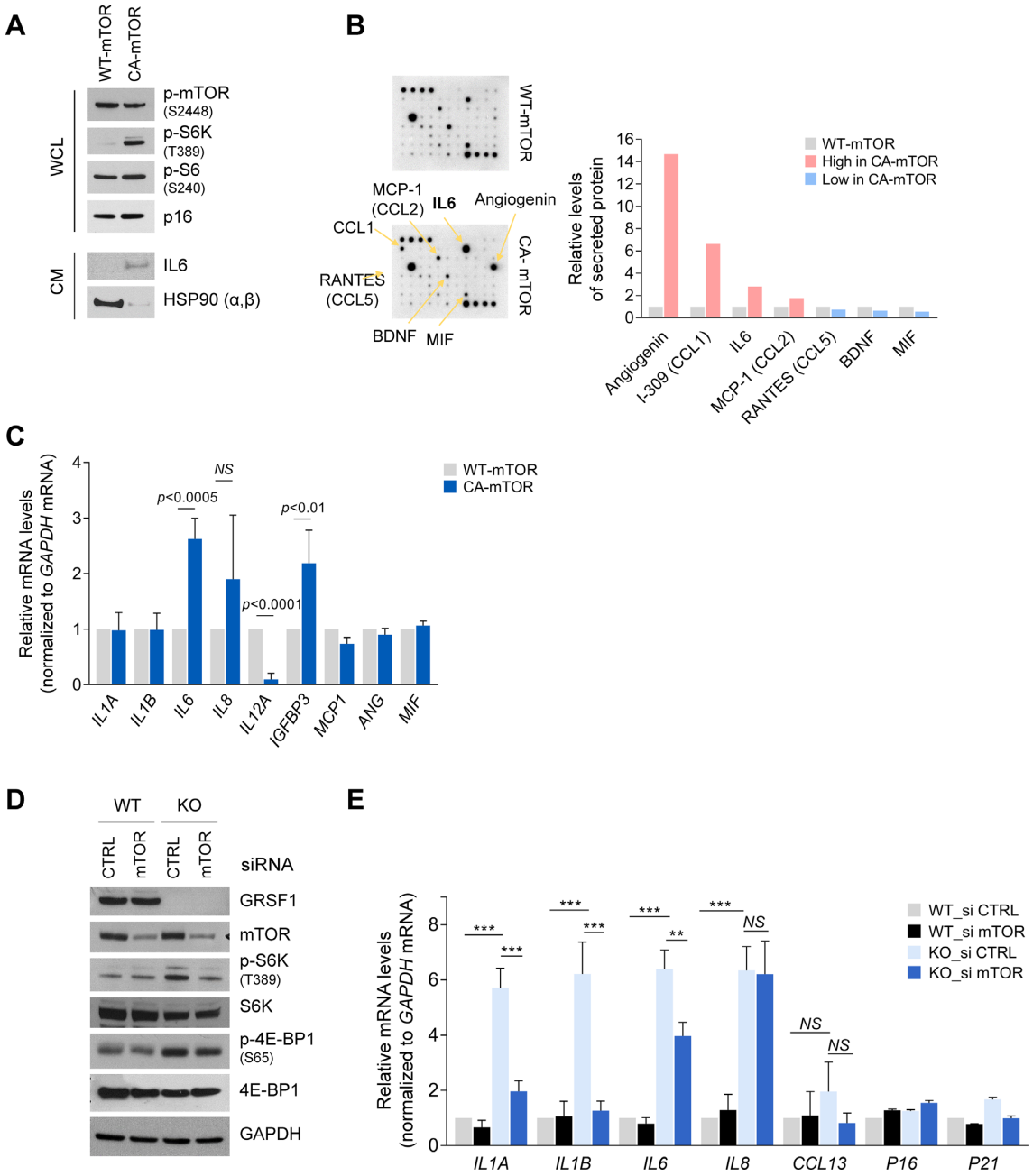

Figure 4. The rise in production of IL6 and cytokines by ablating GRSF1 is largely dependent on mTOR. (**A**–**C**) Plasmid vectors expressing WT mTOR or constitutively active (CA) mTOR were transfected into GRSF1 KO HEK293 cells; 24 h later, Rapamycin was added for an additional 18 h, and 48 h post-transfection, the protein and RNA were analyzed. WCL were used for Western blot analysis, including the analysis of several phosphorylated (p-) proteins (A). CM was also collected from the transfected and serum-starved cells in the presence of Rapamycin, and was used to determine IL6 levels by Western blotting (A) and antibody array analysis (*left*) and quantification (*right*) (B). Total RNA was used to determine the levels of mRNAs encoding cytokines by RT-qPCR analysis (C). (**D**, **E**) WT and KO HEK293 cells were transfected with small interfering (si)RNAs (CTRL or directed to mTOR); 48 h later proteins and RNA were isolated and assessed by Western blotting (D) and RT-qPCR (E) analysis, respectively. The data in (C, E) are the means and ± SD of 3 independent experiments. In (E), $^{**}P < 0.005$; $^{***}P < 0.0001$; NS, not significant.

markedly more abundant in GRSF1 KO cells, this increase was abrogated if NF-κB p65 was silenced (Figure 5C). Collectively, these findings indicate that loss of GRSF1 elevated the expression of cytokines, and that this rise was dependent on the presence of the transcription factor NF-κB p65.

Employing biological replicates of WT and KO HEK293 cells, microarray analysis (Arraystar Inc.) was used to study globally how GRSF1 affected the production of cytokine mRNAs (Materials and Methods). Consistent with the above results, *IL6* mRNA was higher in KO relative to WT HEK293 cells (arrowhead, Figure 5D), while Gene Ontology (GO) analysis uncovered many differentially expressed genes implicated in extracellular pathways (Figure 5E). In addition, many mRNAs known to be transcription-

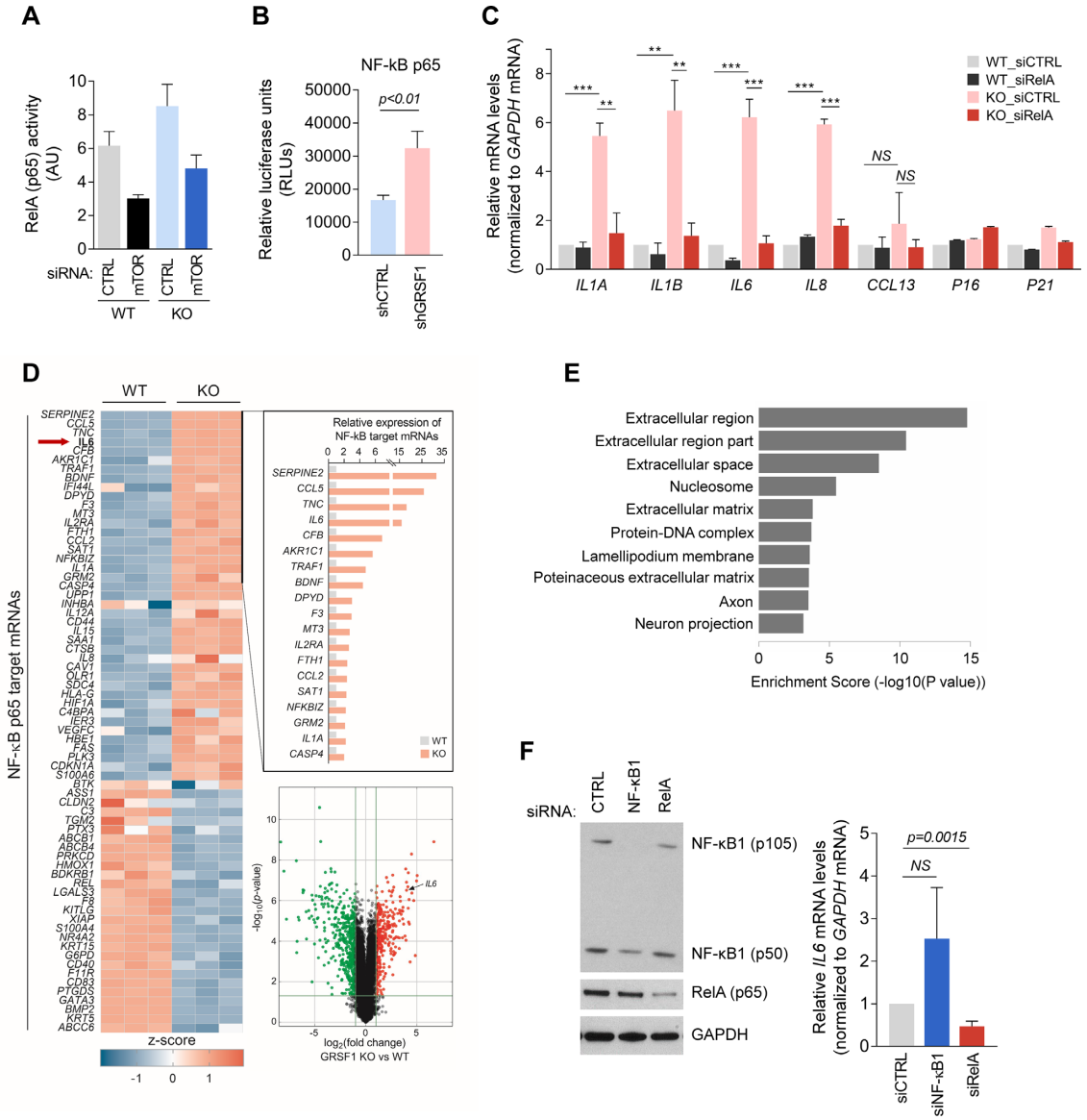

Figure 5. Elevated production of IL6 and other cytokines following GRSF1 ablation is largely dependent on NF-κB activity. (**A**) Forty-eight hours after transfecting HEK293 cells as explained in Figure 4D, nuclei were fractionated and NF-κB p65 (RelA) activity was determined by an ELISA-based assay (Materials and Methods). (**B**) Lentiviruses expressing shGRSF1 or shCTRL were introduced into HEK293 cells stably expressing a luciferase (Luc) reporter gene under transcriptional control of an NF-κB p65-responsive element, and the luciferase activity was determined. (**C**) WT and KO HEK293 cells were transiently transfected with control or NF-κB p65 (RelA)-directed siRNA; 48 h later, the levels of mRNAs encoding cytokines and other factors were determined by RT-qPCR analysis. (**D**) Following microarray analysis (Arraystar) of total RNA in WT and KO HEK293 cells (3 biological replicates per group), differentially expressed mRNAs that were transcriptional targets of NF-κB p65 were clustered (heat map); inset, relative expression levels of the top 19 mRNAs more highly expressed in KO than in WT (*top right*). mRNAs showing statistically significant increases or decreases (fold change ≥ 2 and *P-value* ≤ 0.05) were visualized by Volcano plot; *IL6* mRNA is indicated (*bottom right*). (**E**) A gene set analysis was performed, and the cellular pathways that are highly enriched under GRSF1-deficiency are listed. (**F**) Forty-eight hours after silencing NF-κB1 or RelA in KO cells, the levels of *IL6* mRNA were quantified by RT-qPCR analysis. Data in (A–C) and (F) are the means and ± SD of three independent experiments; $^{**}P < 0.005$; $^{***}P < 0.0001$; NS, not significant. Microarray analysis was performed in triplicate.

ally regulated by NF-κB p65/RelA were differentially up- or downregulated ≥2-fold ($P \leq 0.05$) after GRSF1 loss; the levels of mRNAs encoding pro-inflammatory cytokines (*IL1A*, *IL12A* and *IL15* mRNAs) and chemokines (*CCL5* [*RANTES*], *CCL2* [*MCP-1*], and *CXCL8* mRNAs) were also higher in GRSF1 KO cells (Figure 5D). In particular, the effect of NF-κB on *IL6* mRNA production was specifically dependent on RelA, as silencing NF-κB1 (p105/p50) (Figure 5F, *left*) did not lower *IL6* mRNA levels, only silencing RelA reduced *IL6* mRNA abundance (Figure 5F, *right*). Together, these data indicate that GRSF1 ablation activates mTOR and NF-κB (p65), in turn elevating the production and secretion of cytokines including IL6.

Loss of GRSF1 increases NF-κB-regulated *IL6* mRNA transcription, promotes IL6 translation

The rise in *IL6* mRNA production in KO cells observed above (Figures 4E, 5C and D) was confirmed by additional microarray analysis (Supplemental Figure S3). This increase was at least in part transcriptional, since RT-qPCR analysis revealed a rise in *IL6* pre-mRNA levels (a surrogate measure of nascent transcription) after GRSF1 loss (Figure 6A). Transcription of *IL6* mRNA was further assessed by labeling newly synthesized RNA metabolically in the presence of 4-thiouridine (4-SU) added to the culture medium over the course of 2 h. Following biotinylation on the 4-SU residue, nascent RNA was separated using streptavidin beads and nascent *IL6* mRNA and nascent *GAPDH* mRNA (for normalization) were quantified by RT-qPCR analysis. The results, shown in Figure 6B, indicated a higher rate of *IL6* transcription in GRSF1-deficient cells most apparent at 30 and 45 min.

Moreover, *IL6* mRNA was not stabilized by GRSF1 depletion, as determined by inhibiting *de novo* transcription using actinomycin D and assessing the rate of *IL6* mRNA loss (Figure 6C); as shown, the relative stability of *IL6* mRNA was comparable between WT and KO cells, with apparent half-lives of ∼3 h. Other transcripts analyzed included *IL1A* mRNA, which was also short-lived in both WT and KO cells, *IL1B* mRNA, which was more stable in KO cells, and control transcript *ACTIN* (*ACTB*) mRNA, which is known to be long-lived and encodes a housekeeping protein β-Actin (Figure 6C). The specific mechanisms whereby GRSF1 silencing elevated *IL1A* mRNA without stabilization and rendered *IL1B* mRNA more stable are unknown at present. These data indicate that GRSF1 prevents the production of inflammatory genes and further suggest that the mitochondrial homeostasis maintained by GRSF1 is directly connected to a transcriptional program that includes production of *IL6* mRNA.

To study if the robust rise in IL6 production might also be controlled at the level of translation, cytoplasmic lysates from WT and KO HEK293 cells were fractionated through sucrose gradients into unbound RNA (fractions 1, 2), ribosomal subunits and monosomes (fractions 3, 4), and low- and high-molecular-weight polysomes (LMWP and HMWP, fractions 5–12) (Figure 7A, *left*). After isolating RNA from each fraction and measuring the relative (%) levels of *IL6* mRNA across the gradient, *IL6* mRNA was found to associate with larger polysomes in KO than WT cells (Figure 7A, *right*), consistent with more active translation of IL6 in GRSF1 KO cells. Addition of Rapamycin for 24 h (50 nM) before cells were harvested for polysome fractionation did not restore the level of translation in KO cells to those seen in WT cells (Figure 7B), nor did it change the levels of IL6 produced in either cell line (Figure 7C), suggesting that the translational upregulation of IL6 by loss of GRSF1 was largely mTOR-independent. Although loss of GRSF1 elevated *IL6* mRNA levels dramatically, treatment with Rapamycin did not significantly alter *IL6* mRNA abundance (Supplementary Figure S4). These results were unexpected, given that mTOR signaling promotes general protein translation, and selectively elevates IL1-arm cytokines under NF-κB transcriptional activity (27).

In summary, we propose that in conditions of low or absent GRSF1, reduced activities of Complexes I and IV and NAD+/NADH ratios, as well as increased ROS jointly lead to a rise in DNA damage (Figure 7D). The ensuing DDR activates mTOR and NF-κB and enhance the transcription of *IL6* mRNA, and as-yet unknown mechanisms elevate IL6 translation, jointly rising IL6 secretion.

DISCUSSION

We report evidence that GRSF1 critically controls the production of proteins essential for mitochondrial function, including those required for the function of mitochondrial complexes I and IV (Figure 2). Accordingly, loss of GRSF1 impaired mitochondrial oxidative phosphorylation and elevated ROS, triggering a DNA damage response that in turn activated mTOR and NF-κB, and increasing the production and secretion of pro-inflammatory factors, notably IL6 (Figure 7D). Given this evidence, we propose that the loss of GRSF1 observed in senescent cells contributes to the senescence-associated rise in oxidative stress, DNA damage, growth arrest, and IL6 production (18).

The present study is the first to report that loss of GRSF1 activates mTOR, a kinase that translates nuclear damage into signals and that induce the secretion of IL1-dependent cytokines including IL6 (24,28). A positive feedback loop of paracrine signaling is likely reinforced by an IL6-mediated activation of STAT3 levels and phosphorylation in GRSF1-depleted cells (not shown). Interestingly, several types of mitochondrial dysfunction, including depletion of sirtuins (SIRT3, SIRT5) and chaperones (HSPA), blockage of the electron transport chain, and exhaustion of mtDNA, lack the expression of 'IL1 arm' genes, even when nuclear DNA damage occurs. In addition, the mitochondrial dysfunction-associated senescence (MiDAS) phenotype, characterized by reduced NAD+/NADH, active AMPK and p53, and growth arrest, does not require mTOR activation (29). Therefore, the discovery that GRSF1 elevates IL6 production through mTOR-dependent and -independent pathways suggests that the cell ensures robust IL6 production through different pathways. Moreover, the production of proinflammatory cytokines, including IL6, has been proposed to occur through two separate pathways, perhaps mutually exclusive, one triggered by mitochondrial dysfunction, the other by DNA damage (27). However, our study suggests that the two processes may be simultaneously active via mediators such as GRSF1 that control both pathways.

Efforts to ablate GRSF1 selectively in different mouse tissues are underway, with the goal of elucidating how the ensuing mitochondrial dysfunction, DNA damage, and proinflammatory state impact upon physiology. Along these lines, we anticipate that the generation of mice in which GRSF1 is ablated in muscle and brain, two organs with high energy requirements, will be particularly illuminating. Other ongoing studies are aimed at identifying comprehensively the RNA targets of GRSF1, coding and noncoding, as well as its post-transcriptional function in mitochondria; this work will complement a recent report of GRSF1 target RNAs bearing G-quadruplexes (30). The control of mitochondria-associated gene expression programs by

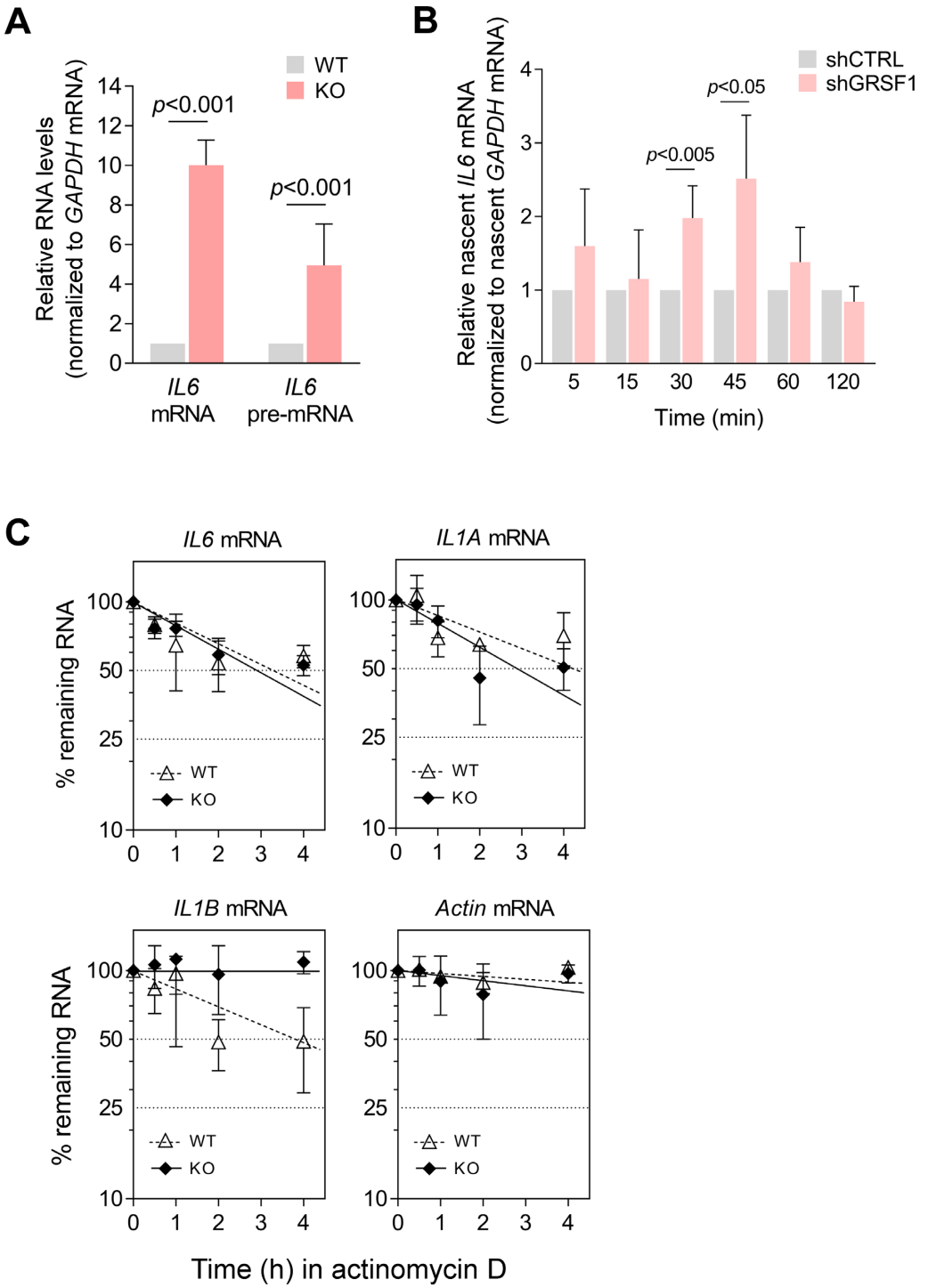

Figure 6. Ablation of GRSF1 increases *IL6* mRNA production transcriptionally. (**A**) The relative levels of *IL6* mRNA and pre-mRNA were quantified by RT-qPCR analysis in WT and KO HEK293 cells. (**B**) Nascent *IL6* pre-mRNA was quantified by incubating WT and KO cells with 4-SU over a range of times (5 min to 2 h) to label newly transcribed RNA; after biotinylating 4-SU residues and purifying biotinylated, 4-SU-labeled RNA was isolated using streptavidin beads. Newly transcribed *IL6* mRNA and newly transcribed *GAPDH* mRNA (for normalization) were quantified by RT-qPCR analysis. (**C**) The relative stabilities of *IL6*, *IL1A*, and *IL1B* mRNAs, as well as a control stable transcript (*ACTIN* mRNA), in WT and KO cells was assessed by incubating cells with actinomycin D for the times indicated, whereupon total RNA was isolated, and the levels of each mRNAs quantified by RT-qPCR analysis and normalized to *18S* rRNA levels. Data in A-C are the means and ± SD of three independent experiments.

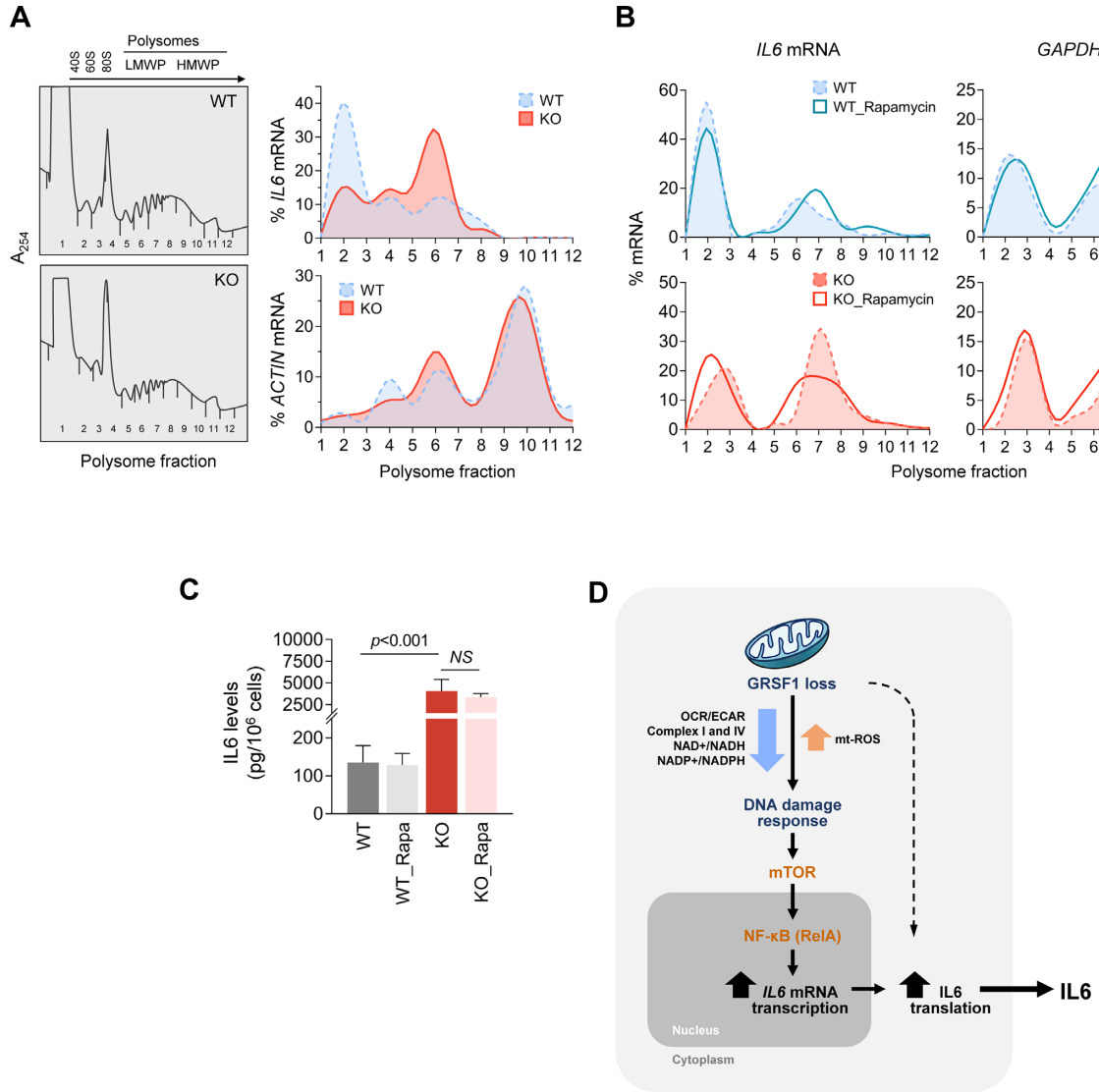

Figure 7. IL6 translation in GRSF1 KO cells is enhanced largely independently of mTOR. (**A**) WT and KO HEK293 cells were harvested and cytoplasmic extracts were sedimented by centrifugation through sucrose density gradients; global polysome profiles depict ribosomal subunits (40S, 60S), and monosomes (80S) as well as low- and high-molecular weight polysomes (LMWP, HMWP) (*left*). RNA was isolated from equal volumes of each fraction, and the presence of *IL6* and *ACTIN* mRNAs was quantified by RT-qPCR analysis and represented as % of the total mRNA on the gradient (*right*). (**B**) Extracts were prepared and processed as in (A), but WT or KO cells were collected after either no treatment or treatment with Rapamycin (Rapa). (**C**) IL6 secreted by untreated and Rapamycin-treated KO and WT cells was quantified by AlphaLISA; data represent the means ± SD from three independent experiments. (**D**) Proposed model. Loss of GRSF1 impairs mitochondrial gene expression programs and mitochondrial function; the ensuing rise in ROS causes DNA damage and triggers a DNA damage response that includes activation of the transcription factor NF-κB and the transcriptional induction in *IL6* mRNA levels. Translation of IL6 is selectively increased in a GRSF1-dependent manner, but this increase appears mTOR-independent.

GRSF1 will be instrumental towards understanding how loss of GRSF1 influences so profoundly the expression patterns of mitochondrial proteins, and hence mitochondrial function (Figure 2). In this regard, it was recently shown that reduced levels of another mitochondrial RBP, the pentatricopeptide repeat domain 1 protein (PTCD1), impaired mitochondrial RNA processing, activated mTOR, and caused metabolic dysfunction in mice including liver steatosis and cardiac hypertrophy (31). These processes were associated with a rise in IL6 following PTCD1 depletion (31). Together with our findings on GRSF1, these studies indicate that the homeostatic control of mitochondrial RNA by RBPs critically preserves tissue function, thereby preventing age-associated decline and disease.

There are numerous therapeutic efforts aimed at neutralizing IL6 function. During early phases of infectious inflammation, IL6 is produced by monocytes and macrophages following stimulation of Toll-like receptors, TLRs (32). In noninfectious inflammation (e.g. following traumatic injury), damage-associated molecular patterns (DAMPs) or dying cells stimulate TLRs to produce IL6 (33). The acute rise in IL6 expression levels stimulates various cell populations, in turn activating the host defense. Once the stress trigger is removed, the signal transduction cascade mediated by IL6 is rapidly eliminated by a regulatory system

that lowers IL6 serum levels (34). The persistent elevation in IL6 production, however, has been implicated in several autoimmune conditions, chronic inflammatory diseases, and cancer (32,35). Given the pathologies associated with elevated IL6, reducing IL6 production or function represents a promising strategy. It will be important to investigate if ectopically raising GRSF1 levels or function can selectively reduce IL6 production. In addition, while the molecular mechanisms that control the levels or mitochondrial localization of GRSF1 are unknown at present, identifying the regulatory factors involved may have therapeutic value. Likewise, identifying chemical compounds that enhance GRSF1 function might be beneficial when aiming to lower IL6 production. Finally, eliminating cells in which declining GRSF1 function has caused a rise in IL6 secretion may also enable a positive outcome. In this regard, eradicating senescent cells through the use of *senolytic* drugs, for example, may help reduce the damage of a persistent proinflammatory state characterized by elevated IL6, and thereby restore tissue and organ homeostasis.

SUPPLEMENTARY DATA

Supplementary Data are available at NAR Online.

ACKNOWLEDGEMENTS

Author Contributions: J.H.N. conceived the study; J.H.N. and K.M.K. designed experiments; J.H.N., K.M.K., P.R.P., N.N.H. and R.M. performed and analyzed experiments; J.L.M., and X.Y. provided technical support; G.K. and S.D. performed informatics analysis; K.A. and M.K.E. contributed intellectually; K.M.K. and M.G. helped with manuscript preparation; and J.H.N and M.G. wrote the manuscript.

FUNDING

National Institute on Aging Intramural Research Program project number [Z01-AG000394-12], NIH. The open access publication charge for this paper has been waived by Oxford University Press - *NAR* Editorial Board members are entitled to one free paper per year in recognition of their work on behalf of the journal.
Conflict of interest statement. None declared.

REFERENCES

1. Glisovic,T., Bachorik,J.L., Yong,J. and Dreyfuss,G. (2008) RNA-binding proteins and post-transcriptional gene regulation. *FEBS Lett.*, **582**, 1977–1986.
2. Dreyfuss,G., Kim,V.N. and Kataoka,N. (2002) Messenger RNA binding proteins and the messages they carry. *Nat. Rev. Mol. Cell Biol.*, **3**, 195–205.
3. Gerstberger,S., Hafner,M. and Tuschl,T. (2014) A census of human RNA-binding proteins. *Nat. Rev. Genet.*, **15**, 829–845.
4. Keene,J.D. (2007) RNA regulons: coordination of posttranscriptional events. *Nat. Rev. Genet.*, **8**, 533–543.
5. Moore,M.J. (2005) From birth to death: the complex lives of eukaryotic mRNAs. *Science*, **309**, 1514–1518.
6. Ivanov,P. and Anderson,P. (2013) Post-transcriptional regulatory networks in immunity. *Immunol. Rev.*, **253**, 253–272.
7. Bisogno,L.S. and Keene,J.D. (2017) RNA regulons in cancer and inflammation. *Curr. Opin. Genet. Dev.*, **48**, 97–103.
8. Wurth,L. and Gebauer,F. (2015) RNA-binding proteins, multifaceted translational regulators in cancer. *Biochim. Biophys. Acta*, **1849**, 881–886.
9. Nishida,K., Kuwano,Y., Nishikawa,T., Masuda,K. and Rokutan,K. (2017) RNA binding proteins and genome integrity. *Int J Mol Sci.*, **18**, E1341.
10. Abdelmohsen,K., Kuwano,Y., Kim,H.H. and Gorospe,M. (2008) Posttranscriptional gene regulation by RNA-binding proteins during oxidative stress: implications for cellular senescence. *Biol. Chem.*, **389**, 243–255.
11. Wang,W. (2012) Regulatory RNA-binding proteins in senescence. *Ageing Res. Rev.*, **11**, 485–490.
12. Harvey,R., Dezi,V., Pizzinga,M. and Willis,A.E. (2017) Post-transcriptional control of gene expression following stress: the role of RNA-binding proteins. *Biochem. Soc. Trans.*, **45**, 1007–1014.
13. Sun,N., Youle,R.J. and Finkel,T. (2016) The mitochondrial basis of aging. *Mol. Cell*, **61**, 654–666.
14. Chan,D.C. (2006) Mitochondria: dynamic organelles in disease, aging, and development. *Cell*, **125**, 1241–1252.
15. Jourdain,A.A., Koppen,M., Wydro,M., Rodley,C.D., Lightowlers,R.N., Chrzanowska-Lightowlers,Z.M. and Martinou,J.C. (2013) GRSF1 regulates RNA processing in mitochondrial RNA granules. *Cell Metab.*, **17**, 399–410.
16. Antonicka,H., Sasarman,F., Nishimura,T., Paupe,V. and Shoubridge,E.A. (2013) The mitochondrial RNA-binding protein GRSF1 localizes to RNA granules and is required for posttranscriptional mitochondrial gene expression. *Cell Metab.*, **17**, 386–398.
17. Noh,J.H., Kim,K.M., Abdelmohsen,K., Yoon,J.H., Panda,A.C., Munk,R., Kim,J., Curtis,J., Moad,C.A., Wohler,C.M. *et al.* (2016) HuR and GRSF1 modulate the nuclear export and mitochondrial localization of the lncRNA RMRP. *Genes Dev.*, **30**, 1224–1239.
18. Noh,J.H., Kim,K.M., Idda,M.L., Martindale,J.L., Yang,X., Abdelmohsen,K. and Gorospe,M. (2018) GRSF1 suppresses cell senescence. *Aging*, **10**, 1856–1866.
19. Kim,K.M., Noh,J.H., Bodogai,M., Martindale,J.L., Pandey,P.R., Yang,X., Biragyn,A., Abdelmohsen,K. and Gorospe,M. (2018) SCAMP4 enhances the senescent cell secretome. *Genes Dev.*, **32**, 909–914.
20. Trzeciak,A.R., Barnes,J. and Evans,M.K. (2008) A modified alkaline comet assay for measuring DNA repair capacity in human populations. *Radiat Res.*, **169**, 110–121.
21. Hirst,J. (2013) Mitochondrial complex I. *Annu. Rev. Biochem.*, **82**, 551–575.
22. Schindler,C., Levy,D.E. and Decker,T. (2007) JAK-STAT signaling: from interferons to cytokines. *J. Biol. Chem.*, **282**, 20059–20063.
23. Weichhart,T., Hengstschläger,M. and Linke,M. (2015) Regulation of innate immune cell function by mTOR. *Nat. Rev. Immunol.*, **15**, 599–614.
24. Laberge,R.M., Sun,Y., Orjalo,A.V., Patil,C.K., Freund,A., Zhou,L., Curran,S.C., Davalos,A.R., Wilson-Edell,K.A., Liu,S. *et al.* (2015) MTOR regulates the pro-tumorigenic senescence-associated secretory phenotype by promoting IL1A translation. *Nat. Cell Biol.*, **17**, 1049–1061.
25. Kapahi,P., Chen,D., Rogers,A.N., Katewa,S.D., Li,P.W., Thomas,E.L. and Kockel,L. (2010) With TOR, less is more: a key role for the conserved nutrient-sensing TOR pathway in aging. *Cell Metab.*, **11**, 453–465.
26. Liu,T., Zhang,L., Joo,D. and Sun,S.C. (2017) NF-κB signaling in inflammation. *Signal Transduct. Target Ther.*, **2**, 17023.
27. Fernandez-Marcos,P.J. and Serrano,M. (2016) Mitochondrial damage induces senescence with a twisted arm. *Cell Metab.*, **23**, 229–230.
28. Herranz,N., Gallage,S., Mellone,M., Wuestefeld,T., Klotz,S., Hanley,C.J., Raguz,S., Acosta,J.C., Innes,A.J., Banito,A *et al.*2015) mTOR regulates MAPKAPK2 translation to control the senescence-associated secretory phenotype. *Nat. Cell Biol.*, **17**, 1205–1217.
29. Wiley,C.D., Velarde,M.C., Lecot,P., Liu,S., Sarnoski,E.A., Freund,A., Shirakawa,K., Lim,H.W., Davis,S.S., Ramanathan,A. *et al.* (2016) Mitochondrial dysfunction induces senescence with a distinct secretory phenotype. *Cell Metab.*, **23**, 303–314.
30. Pietras,Z., Wojcik,M.A., Borowski,L.S., Szewczyk,M., Kulinski,T.M., Cysewski,D., Stepien,P.P., Dziembowski,A. and

Szczesny,R.J. (2018) Dedicated surveillance mechanism controls G-quadruplex forming non-coding RNAs in human mitochondria. *Nat. Commun.*, **9**, 2558.
31. Perks,K.L., Ferreira,N., Richman,T.R., Ermer,J.A., Kuznetsova,I., Shearwood,A.J., Lee,R.G., Viola,H.M., Johnstone,V.P.A., Matthews,V. *et al.* (2017) Adult-onset obesity is triggered by impaired mitochondrial gene expression. *Sci. Adv.*, **3**, e1700677.
32. Tanaka,T., Narazaki,M. and Kishimoto,T. (2014) IL-6 in inflammation, immunity, and disease. *Cold Spring Harb. Perspect. Biol.*, **6**, a016295.
33. Anders,H.J. and Schaefer,L. (2014) Beyond tissue injury-damage-associated molecular patterns, toll-like receptors, and inflammasomes also drive regeneration and fibrosis. *J. Am. Soc. Nephrol.*, **25**, 1387–1400.
34. Ahmed,S.T. and Ivashkiv,L.B. (2000) Inhibition of IL-6 and IL-10 signaling and Stat activation by inflammatory and stress pathways. *J. Immunol.*, **165**, 5227–5237.
35. Taniguchi,K. and Karin,M. (2014) IL-6 and related cytokines as the critical lynchpins between inflammation and cancer. *Semin. Immunol.*, **26**, 54–74.